ACS OMEGA

http://pubs.acs.org/journal/acsodf

Article

Buried-Gate MWCNT FET-Based Nanobiosensing Device for Real-Time Detection of CRP

Ali Firoozbakhtian, Ali Hossein Rezayan,* Hassan Hajghassem, Fereshteh Rahimi, Masoud Faraghi Ghazani, Mahsa Kalantar, and Amir Mohamadsharifi

Cite This: *ACS Omega* 2022, 7, 7341−7349

Read Online

ACCESS | Metrics & More | Article Recommendations | Supporting Information

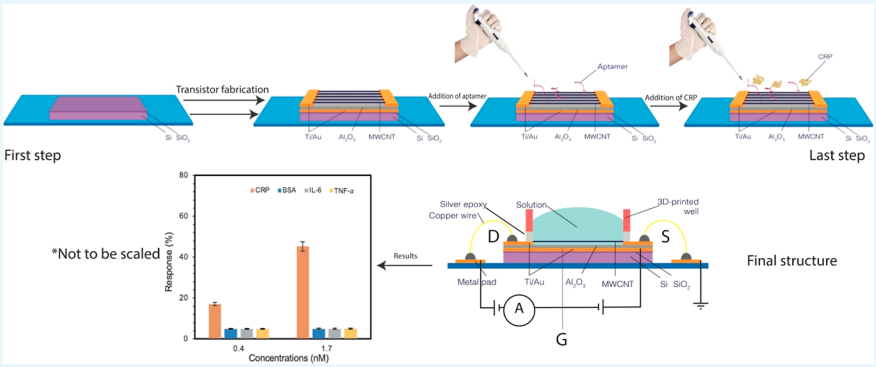

ABSTRACT: C-reactive protein (CRP), an acute-phase protein synthesized in the liver in response to inflammation, is one of the biomarkers used for the detection of several diseases. Sepsis and cardiovascular diseases are two of the most important diseases for which detection of CRP at very early stages in the clinical range can help avert serious consequences. Here, a CNT-based nanobiosensing system, which is portable and reproducible, is used for label-free, online detection of CRP. The system consists of an aptameric CNT-based field-effect transistor benefiting from a buried gate geometry with Al_2O_3 as a high dielectric layer and can reflect the pro-cytokine concentration. Test results show that the device responds to CRP changes within 8 min, with a limit of detection as low as 150 pM (0.017 mg L^{-1}). The device was found to have a linear behavior in the range of 0.43−42.86 nM (0.05−5 mg L^{-1}). The selectivity of the device was tested with TNF-α, IL-6, and BSA, to which the nanosensing system showed no significant response compared with CRP. The device showed good stability for 14 days and was completely reproducible during this period. These findings indicate that the proposed portable system is a potential candidate for CRP measurements in the clinical range.

INTRODUCTION

C-reactive protein (CRP) is an acute phase protein produced by the liver in response to inflammation or in the cases of cardiovascular diseases.[1−4] The levels of CRP corresponding to inflammation indicate that a concentration of 2 mg L^{-1} or less is among the normal concentrations, while in the case of inflammation, the levels can rise up to 1000-fold.[5] The reported concentrations in septic patients range from 12 to 159 mg L^{-1}, which exhibits a significant overlap with the 13−119 mg L^{-1} range in systemic inflammatory response syndrome patients.[6,7] The concentrations in the case of cardiovascular diseases are rather classified differently and fall into three categories. A concentration of less than 1 mg L^{-1} is considered to be normal, the low-risk group lies between 1 and 3 mg L^{-1}, and concentrations higher than 3 mg L^{-1} are considered to be of high risk.[8,9] Since CRP aids in the phagocytosis of bacteria, its levels augment late during the onset of sepsis.[10] Thus, early diagnosis in conjunction with appropriate treatment can help avert the serious and sometimes deadly consequences. It should be noted that CRP is not considered as a specific biomarker; however, it provides useful information to the health practitioner as to whether inflammation or cardiovascular disease is present.[11] For example, a CRP concentration of >8.7 mg dL^{-1} and a temperature of more than 38.2 °C were associated with infection with sensitivities of 93.4 and 54.8% and specificities of 86.1 and 88.9%, respectively.[12] Currently, CRP analysis is done by assays of turbidimetry, nephelometry, and enzyme-linked immunoassay, with the latter being considered as the gold standard for this diagnosis.[13−15] These assays also have disadvantages of being expensive, time-consuming, not sensitive enough, and being prone to false

Received: December 24, 2021
Accepted: February 1, 2022
Published: February 14, 2022

https://doi.org/10.1021/acsomega.1c07271
ACS Omega 2022, 7, 7341−7349

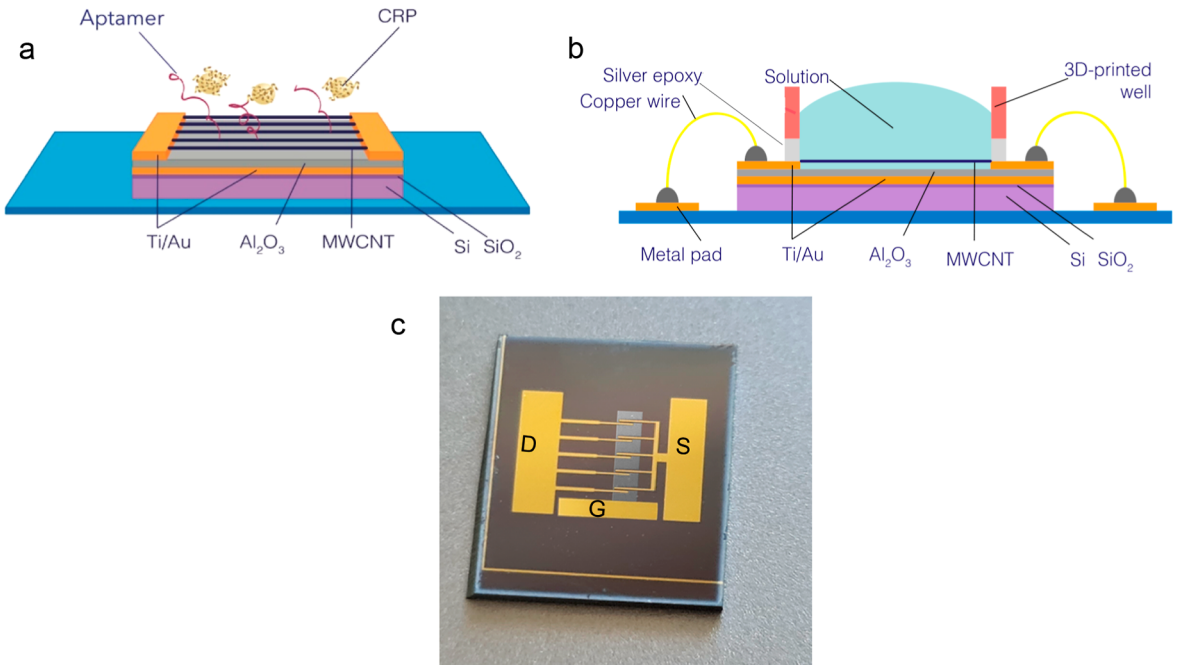

Figure 1. (a) Schematic of the aptameric MWCNTFET biosensor. The device benefits from a buried gate geometry for the detection of CRP. (b) Schematic of the FET-based nanobiosensor. The 3D-printed well is mounted on the sensing area, making liquid handling easier. The source, drain, and gate electrodes are connected to the power supplier with a copper wire. (c) Photograph of a MWCNTFET nanosensor before the immobilization of MWCNTs. The buried gate geometry is covered with a 40 nm thick layer of Al_2O_3 (in gray) acting as a high-κ dielectric. A titanium/gold contact is seen and labeled as G, which is connected to the power supply through a copper wire. The MWCNTs' conducting channel connects the drain and source electrodes, and the gate electrode which has the same constituents as the drain and source is buried under a 40 nm thick layer of Al_2O_3.

results.[16,17] The disadvantages of these techniques continue since they need skilled personnel and sophisticated equipment and therefore cannot be performed in remote areas.[18] The quantification methods reported to date are surface plasmon resonance and surface-enhanced Raman scattering,[19,20] microfluidic devices,[21] quartz crystal microbalance technology,[22−25] electrochemistry,[26−28] and field-effect transistor (FET)-based biosensors.[29−31] Among these techniques, electrochemistry and FET-based devices have shown the good features of inexpensiveness, flexibility, sensitivity, and rapidness in terms of producing results. The use of gold nanorods in conjunction with antibody receptors accounted for a limit of detection of 10 fM in the paper published by Letchumanan et al.[17] Vilian et al. used an electron-mediated electrochemical device for the fast detection of CRP, which works in a linear range of 5−220 fg mL^{-1}.[2] In another study, a CRP electrochemical biosensor consisting of an eight Ag ion-intercalated multifunctional DNA four-way junction (MF-DNA-4WJ) and a porous rhodium nanoparticle (pRhNP) heterolayer on a microgap electrode was fabricated by Kim et al.,[32] which was able to detect a concentration as low as 0.349 pM.

It has not been until recently that the FET-based biosensors (aka. BioFETs) have been recognized as fast, infallible, compact, power-efficient, and extremely sensitive. The use of BioFETs in the biosensor industry has also addressed a rather important issue caused by the introduction of labels to the target molecules since it provides label-free detection of biomolecules. For example, there has been numerous reports of high-electron-mobility transistor (HEMT)-type FET sensors for chemical and biological applications.[33−35] Kim et al.[36] developed an extended gate FET-based biosensor for the detection of streptavidin−biotin protein complexes. Tans et al.[37] have reported the use of carbon nanotubes (CNTs) as channels in CNTFETs. Owing to their special geometry and high surface to volume ratio, CNTs have become a good candidate to be used in highly sensitive nanobiosensors. The use of CNT-based FETs (CNTFETs) in biosensing has been the center of attention for their high sensitivity and selectivity, no need for labeling, real-time sample measurements, rapidness, flexibility, and the low cost of fabrication. The conductance of these devices changes by the charge transfer from the molecules absorbed onto their surfaces.[38−40] In these sensing platforms, the CNT surface is functionalized with bioreceptors capable of attaching to the biomolecule of interest. When the target molecule binds to the bioreceptor in a solution, the charges of the target molecule in the solution affect the conductance of the CNTFET and hence enable the detection. In the presence of a buffer in the solution, a double layer is formed in the range of Debye length around the CNTs.[41,42] The target−receptor complex should fit in the double layer to enable the charge transfers to the CNTs. When a charged biomolecule is absorbed on the surface of the CNTFET channel, a reduction in the source−drain current is seen. Since the diameter of biomolecules is much bigger than the diameter of the CNT channels, we expect them to have high sensitivity for the detection of biomolecules.

Detection of proteins with antibodies is very common. However, the high cost of antibodies, their large size, and low stability have led recent research into using alternatives.[43] Aptamers, artificial oligonucleotides, have gained attention due to their low cost and high stability, and their relatively small size enables detection in the double-layer range.[41,44,45] The good reproducibility seen in the aptasensors is due to their well-established chemical synthesis routes.[46] The binding

https://doi.org/10.1021/acsomega.1c07271
ACS Omega 2022, 7, 7341−7349

affinity to target molecules is almost the same as that of antibodies, hence they are often called chemical antibodies.[47−49] The use of nanostructured gate electrodes and shortness of aptamers help overcome the adverse effects of Debye screening in physiological solutions.[30] Therefore, protein−aptamer reactions happen in the electrical double layer. The small size of aptamers also contributes to their immobilization at a higher density, which would mean a higher sensitivity in detection.[50]

To address the issues impeding the cost effectiveness, sensitivity, and fast detection of CRP and in continuation of our research, especially in the field of biosensors,[51−54] we hereby report a sensitive multiwalled CNTFET (MWCNTFET) sensor, that is small enough and can be easily categorized as a portable device and using aptamers as capture probes for convenient online detection of CRP. The system consists of an aptameric MWCNTFET-based biosensor and a 3D-printed well, mounted on the sensing area for better liquid handling (Figure 1a−c).

EXPERIMENTAL AND METHODS

Chemicals and Materials. MWCNTs functionalized with carboxyl groups were purchased from Sigma-Aldrich (Munich, Germany). 285 nm SiO_2/Si was ordered from Wafer World (West Palm Beach, FL, US). Human CRP was purchased from Sigma-Aldrich (Munich, Germany). Phosphate-buffered saline (PBS) was purchased from Sigma-Aldrich (Munich, Germany). (3-Aminopropyl)triethoxysilane (APTES) was purchased from Sigma-Aldrich (Munich, Germany). Ethanolamine was purchased from Sigma-Aldrich (Munich, Germany). 1-Ethyl-3-(3-dimethylaminopropyl) carbodiimide (EDC) was purchased from Sigma-Aldrich (Munich, Germany). *N*-Hydroxysuccinimide (NHS) was purchased from Sigma-Aldrich (Munich, Germany). The CRP-specific DNA aptamer 5′-NH_2-ACACGATGGGGGGGTATGATTT-GATGTGGTTGTTGCATGATCGTGG-3′) was synthesized and purified by the BIO-RP purification method. Ethanol amine was purchased from Sigma-Aldrich (Munich, Germany).

Nanosensor Fabrication. The 285 nm SiO_2/Si was cleaned successively by acetone, isopropanol, and deionized water. Then, SiO_2/Si was dried and treated with plasma prior to being employed as the substrate of our sensor. The buried gate electrode was forged by the bilayer lift-off photolithography process. The process used two layers of a resist, a sacrificial layer and a photoresist, which were spin-coated using a spin coater. The gate electrode consisting of a Ti/Au structure (50 nm/120 nm) was marked out on the SiO_2/Si substrate using standard photolithography, and the metal deposition was done by the physical vapor deposition technique. A 40 nm thick nanolayer of Al_2O_3 was put on top of our gate electrode as the high-κ dielectric. We then repeated the process of photolithography to fabricate the source and drain electrodes, which were also made out of Ti/Au (50 nm/120 nm) on top of the Al_2O_3 surface. Following the Sputter deposition of the metals, the nanosensor was exposed to oxygen plasma again to remove the remaining residues. Then, N_2 was used to remove any possible dust on the surface of the nanosensor. APTES (5% v/v) was dropped on the surface of the nanosensor and then spin-coated using the spin coater to produce a unified layer on the whole surface. After that, the nanosensor was put into an oven for 20 min at 80 °C in order to activate APTES. The whole purpose of APTES is to activate the surface with amine groups. Figure 2a shows the FTIR spectra after APTES treatment. Carboxylated MWCNTs (0.05 g) were ultrasonicated in a prepared solution of ethanol, NHS (400 mM), and EDC (20 mM) to get them dispersed to their full extent while activating the carboxyl groups on the MWCNTs as well. Figure S2 shows a schematic step-by-step process of the device fabrication. The FTIR spectra of MWCNT COOH functionalized groups are shown in Figure

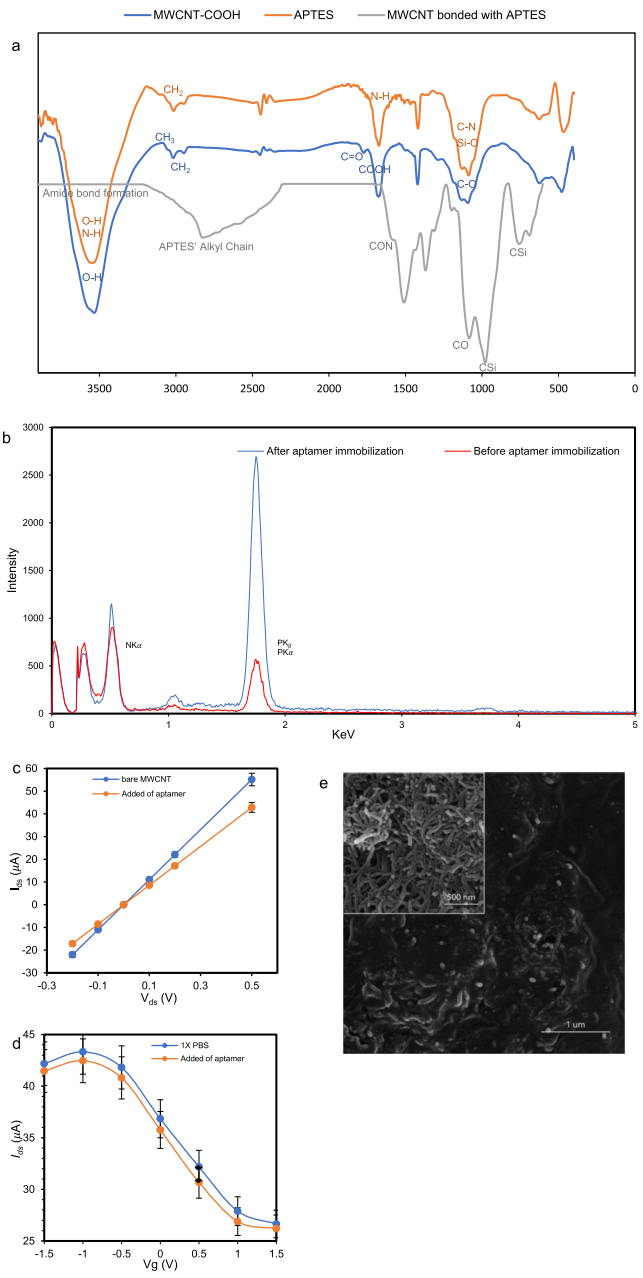

Figure 2. (a) FTIR spectra of the APTES-functionalized surface of Al_2O_3 (orange line). APTES introduces amine groups on the surface. FTIR spectra of COOH-functionalized MWCNTs (green line). ATR-FTIR spectra of immobilized MWCNTs on the APTES-functionalized surface of alumina (blue line). (b) EDX spectra of MWCNTs before and after aptamer immobilization. A sharp increase in the intensities of P and N is seen. (c) Drain−source current as a function of drain−source voltage. (d) Drain−source current plotted against a range of V_g at V_{ds} = 0.2 V. (e) FESEM image of MWCNTs after aptamer immobilization. The diameter of the MWCNTs increased after aptamer immobilization; (inset) FESEM image of the MWCNTs (Figure S3d,e).

https://doi.org/10.1021/acsomega.1c07271
ACS Omega 2022, 7, 7341−7349

2a. The aforementioned MWCNTs were dropped on the nanosensor using a sampler and then were let to rest and form covalent bonds for 2 h at room temperature.

Biochemical Functionalization. To immobilize the aptamers on the MWCNTs, the nanosensor was incubated with 3 μM aptamer solution overnight at room temperature. After rinsing with 1× PBS, 100 mM of ethanolamine was added to the surface of the nanosensor for 90 min to block the excess remaining functional groups on the MWCNT surface. To address the liquid handling problem, a 3D-printed well was carefully placed on the sensing area of our nanosensor.

Preparation of CRP Samples. Buffer dilution reduces the ionic strength of the solution and hence increases the Debye length.[30] Here, we used 1× PBS to dilute our CRP samples and create a dilution series of interest. A dilution range of 0.43−171.43 nM (0.05−20 mg/L) of the protein was prepared. The samples were let to rest overnight and were used the day after. The storage temperature for this step was 4 °C.

Liquid Handling. While testing, a volume of 10 μL CRP at various concentrations is added to and removed from the 3D-printed well using a sampler. No need for rinsing after the removal of the solution was recognized.

RESULTS AND DISCUSSION

Working Principle of the Nanobiosensor. A 40 nm thick layer of Al_2O_3 that works as a high dielectric layer with ε = 11.54 was grown on the gate electrode to insulate it from the MWCNTs. A drain current I_{ds} through the MWCNTs is generated by a drain−source voltage V_{ds}, powered by Rigol (DP821). An external gate voltage V_g was applied at its optimal value, where both the sensor's sensitivity and MWCNT conductivity reached their maximum potentials. The changes of drain−source current I_{ds} were recorded until reaching equilibrium in 8 min. The FET-based biosensor either behaves in a linear region for quantitative analysis or in a subthreshold way for higher sensitivity. The drain current reduces after the immobilization of the ssDNA aptamer due to the interfacial dipole between nucleobases and MWCNTs in addition to $\pi-\pi$ stacking. Density functional theory calculations indicate that the physisorption of DNA induces an interfacial dipole between nucleobases and MWCNTs in addition to $\pi-\pi$ staking.[55] The dipole is the direct result of electron-rich aromatic rings' closure to the polarized MWCNT surface and is responsible for the mobility and density decrease of the electron carriers in the channel.[56,57] The current decrease is due to the depletion of negative charge carriers induced by the aptamer-CRP binding interaction. A schematic of the sensing principle is seen in Figure S1. As can be seen, the aptamers are in an unfolded state in the fresh buffer. Upon introduction of CRP to the environment, the aptamers attach to CRP and become folded, bringing CRP to the vicinity of MWCNTs' surface. The negatively charged protein induces positive charges in the MWCNTs, which leads to an increase in the number of free electron carriers in the MWCNTs and hence a change in the drain current.

Characterization. To assure the successful functionalization, several characterization steps were adopted. ATR−FTIR (Thermo Nicolet Avatar 380) spectra of the Al_2O_3 surface showed the presence of amine groups, which indicates the successful functionalization of the dielectric layer with APTES (Figure 2a). As shown in the spectra, O−H stretching and N−H stretching are seen at 3400 cm^{-1}. The wavenumbers 2920 and 2850 cm^{-1} indicate the existence of asymmetrical/symmetrical stretching in CH_2, respectively. A strong N−H vibrational bending due to the presence of amino groups is seen at 1630 cm^{-1}. 950−1000 cm^{-1} peaks are responsible for C−N and Si−O functional groups and confirm the presence of amine groups.[58] FTIR analysis was also performed on carboxylated MWCNTs to confirm the existence of the carboxyl groups (Figure 2a). An intensive band at 3421 cm^{-1} due to stretching vibrations of isolated surface −OH moieties or −OH in carboxyl groups is seen. Asymmetric methyl stretching and asymmetric/symmetric methylene stretching bands at 2960, 2923, and 2853 cm^{-1} are shown. The C═O bands that are characteristics of carboxyl functional groups are observed at 1732 and 1630 cm^{-1}. Observed at 1380 cm^{-1} is the band responsible for the presence of vibrational bending of C−H. Vibrational stretching of C−O can be seen at 1069 cm^{-1}.[59] ATR−FTIR analysis was performed on the MWCNTs immobilized on the surface of APTES-functionalized alumina to confirm the bonding of carboxy groups on MWCNTs with amine groups of APTES to form an amide bond (Figure 2a). The formation of amide bonds was seen due to the disappearing peaks of OH and NH at 3300−3600 cm^{-1}. The alkyl chain of APTES was seen at 2960 cm^{-1}. The formation of CON bonds between MWCNT-COOH and APTES was seen at 1700 cm^{-1}. Carbonyl functional groups were seen at 1200 cm^{-1}. The formation of CSi bonds was seen at 1000 and 760 cm^{-1}. All these suggest the successful functionalization and immobilization of MWCNTs on the alumina surface.

Energy-dispersive X-ray analysis (EDX) (Thermo scientific K-Alpha+) was performed to confirm the immobilization of aptamers on the MWCNTs. We measured the intensity of nitrogen and phosphorous elements on the MWCNTs' surface before and after aptamer immobilization, which are shown with red and blue lines, respectively. As expected, a sharp rise in the intensity of the P and N elements was seen, which corresponds to the successful immobilization of the ssDNA aptamers (Figure 2b).

I_{ds} was measured before and after aptamer immobilization on the surface. The I_{ds} measured decreased drastically after aptamer immobilization (Figure 2c,d, data shown are an average of the values from five sensors). As shown in the graph, the device demonstrates a fully linear relationship between I_{ds} and V_{ds}, which shows that a fully Ohmic contact between the source and drain exists. In order to find the optimum V_g, the I_{ds} was measured against a range of interest for V_g with steps of 0.1 V. The sweeping of V_g was fast enough to not let the biosensors reach a thermal equilibrium. The drain current reduces as the V_g increases. I_{ds} was measured once with 1× PBS and once after the immobilization of the aptamer. The data showed a maximum difference between I_{ds} measured in the presence of 1× PBS and I_{ds} measured in the presence of the aptamer at V_g = 0.5 V (Figure 2d). Figure S3a,b shows the values obtained for sensors before and after aptamer immobilization.

To further confirm the attachment of aptamers to the MWCNTs' surface, FESEM images (using TESCAN MIRA III) were taken from the MWCNTs before and after aptamer immobilization (Figure 2e). The MWCNTs' diameters show an increase after aptamer immobilization (Figures 2e and a−c). All these experimental results are in consistency with those of An et al.,[60] suggesting the successful immobilization of the aptamer on the MWCNTs' surface.

https://doi.org/10.1021/acsomega.1c07271
ACS Omega 2022, 7, 7341−7349

CRP Detection. The nanobiosensor's detecting capability was tested by exposing the sensing area to CRP artificial sample solutions. The response of the FET-based nanobiosensor is defined as Response = $(I_0 - I_c/I_0) \times 100$, where I_0 is defined as the drain−source current before exposure to protein measured in the fresh PBS buffer and I_c is the drain−source current after protein addition. The sensor's response was evaluated at certain V_{ds} and V_{gs} in the linear working regime. The drain−source current decreases after protein addition and reaches an equilibrium at about 8 min. As can be seen from the formula, the response of the sensor increases with the increasing concentration of CRP. Time-resolved measurements of CRP were performed at fixed V_{ds} = 0.2 V and V_{gs} = 0.5 V in 1× PBS and CRP artificial sample solution. As shown in Figure 3, the response increases sharply from 0 to 95

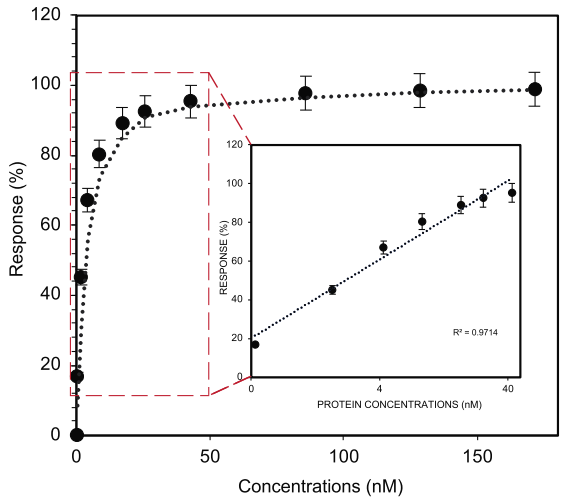

Figure 3. Detection of CRP in artificial samples. Responses produced plotted against the concentration of the CRP. The responses are shown as $\Delta I/I_0$. Inset: responses of the device against the logarithmic concentration of the CRP.

with increasing concentrations of CRP to 43 nM (5 mg L^{-1}). The binding of CRP and its aptamer seems to reach saturation at further concentrations and reaches 98 at 85.71 nM (10 mg L^{-1}). The response of the sensor remains almost unchanged up to 171.43 (20 mg L^{-1}). The inset of Figure 3 shows the responses as a function of the logarithm of protein concentrations. The range of the linear relationship lies between 0.43 and 42.86 nM (0.05−5 mg L^{-1}). The limit of detection calculated based on the $3\sigma/s$ formula[61] was as low as 150 pM (0.017 mg L^{-1}).

As seen in the inset of Figure 3, the first point of the plot indicates a concentration of 0.43 nM (0.05 mg L^{-1}) and the last point shown is a representative for 42.86 nM (5 mg L^{-1}). As can be seen, the device shows a linear relationship between the responses and the logarithm of protein concentration. Responses produced with increasing concentrations after 5 mg L^{-1} cannot be distinguished from one another since they are extremely close. The values plotted here are an average of five devices.

K_d, the binding equilibrium constant, can be determined from the sensor's response. A lower K_d stands for the stronger tendency for the aptamer to bind to CRP. The constant can be calculated from the equation below[62,63]

$$\text{response} = \frac{C_i}{C_i + K_d}$$

where C_i is the concentration of the CRP at which the response is produced. From the above equation, the average K_d of all five sensors was calculated at 2.09 nM, which shows a good sensing performance by the nanosensor through different sample solutions.

Control Experiment and Selectivity. To make sure that the MWCNTs used in this experiment had no affinity for direct CRP bonding, a concentration of CRP of 0.4 nM up to 17.14 nM was added to bare MWCNTs and the response was measured.[64] As shown in Figure 4a, the signal remained constant in the sensing time (8 min). This finding showed that either the CRP has no effects on the bare MWCNTs or the effect is so low that it cannot be detected by our device.

Before aptamer immobilization, the responses produced by the application of a range of CRP concentrations to the surface of the biosensor were measured. The responses changed from 0 to 1% and remained almost constant with increasing concentrations of the protein, indicating that the MWCNTs do not have affinity for the protein of interest and rationalize the choice of them as our conducting channel.

Selectivity of the Nanobiosensor. The selectivity of the nanobiosensor was measured using TNF-α, IL-6, and BSA.

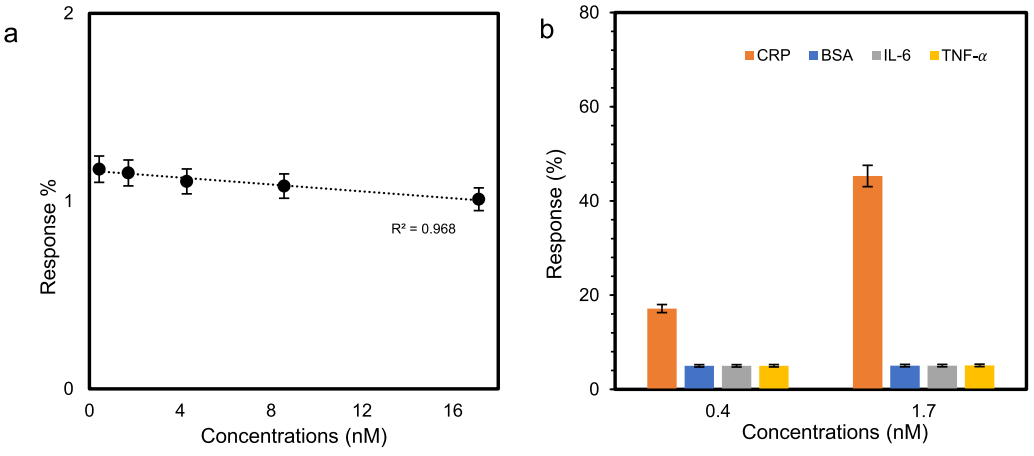

Figure 4. (a) Inertness of bare COOH-functionalized MWCNTs to CRP. (b) Selectivity of the nanobiosensor. Responses of three other proteins are plotted against the response of CRP. The maximum response produced by other proteins is 5.11% by a concentration of 1.7 nM BSA.

https://doi.org/10.1021/acsomega.1c07271
ACS Omega 2022, 7, 7341−7349

TNF-α and IL-6 were chosen since they are also found in the onset of sepsis and their concentrations also rise in response to sepsis. BSA was chosen since albumin is found in a large amount in the body. Figure S6 shows the responses from these three proteins plotted against their concentrations. As can be seen, the responses remain constant and do not change with the increasing concentration of the proteins (the responses did not change from 100 to 2000 pM for the three proteins). The responses recorded from the addition of these proteins at different concentrations are plotted against their concentrations. As shown in Figure 4b, the responses remained constant with the increase in the concentration of the proteins. The changes in the responses were compared to the changes of the responses produced by the same concentration of CRP. The graph shows that the same increase in CRP concentration produced almost 28% more response in comparison with other proteins.

Reproducibility and Stability Tests. In order to measure the reproducibility and stability of the biosensor, a series of identical tests were performed. Responses produced from a series of concentrations of CRP were measured over a course of 18 days. The correlation coefficient was measured for the responses all against those on day 1. The sensor showed stability and precision in the results produced until day 14 (Figure 5).

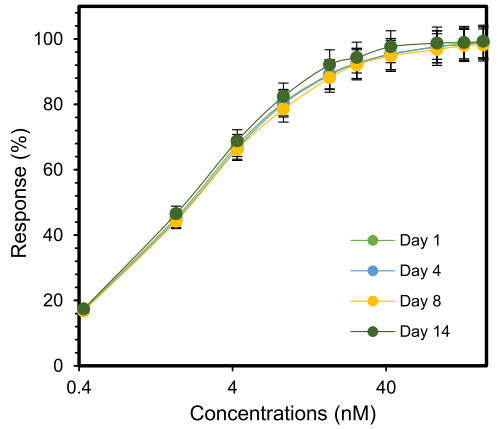

Figure 5. Reproducibility and stability of the biosensor. The responses of the five sensors to a certain series of CRP concentrations. The devices are good to be used until day 14.

Below, a comparison between different methods of detection of CRP with this work is presented. As can be seen from Table 1, the linear range of the sensors reported does not cover the physiological concentration of the protein. Although these sensors can detect very low concentrations, they are not of use in clinical diagnoses.

CONCLUSIONS

Here, an MWCNT FET-based nanobiosensor for real-time detection of CRP is presented. The system consists of an aptameric MWCNT FET nanobiosensor with a buried gate electrode geometry and a 3D-printed well mounted on top of its sensing area for better handling of the samples. The inertness of MWCNTs to CRP was measured with the results justifying the appropriateness of MWCNTs as the conducting channel. No need for a linker to attach aptamers to MWCNTs means that our designed system not only cuts the expenses of a linker but also makes the aptamer−CRP interaction occur closer to the surface of MWCNTs, which leads to a higher sensitivity. The specificity of the sensor was measured through the use of negative controls. Since under the condition of sepsis, the concentrations of IL-6 and TNF-α rise as well, we used these two proteins and BSA as our negative controls. Test results indicated that the sensor is highly specific to CRP and can be relied upon in that manner. The proposed nanobiosensor can respond to CRP concentration changes in 8 min with a limit of detection down to 150 pM (0.017 mg L^{-1}) and a linear range of 0.43−42.86 nM (0.05−5 mg L^{-1}), which covers the physiological level of CRP in the human body. The nanosensing system holds great potential to be used in the clinical diagnosis of CRP-related diseases at very early stages.

ASSOCIATED CONTENT

Supporting Information

The Supporting Information is available free of charge at https://pubs.acs.org/doi/10.1021/acsomega.1c07271.

Principle of CRP detection, nanosensor fabrication, uncorrected FTIR spectra of each modification step, histogram of the diameter distribution of the MWCNTs before and after aptamer immobilization, drain−source current graphs, and plots showing selectivity of the sensor (PDF)

AUTHOR INFORMATION

Corresponding Author

Ali Hossein Rezayan − *Division of Nanobiotechnology, Department of Life Sciences Engineering, Faculty of New Sciences and Technologies, University of Tehran, Tehran 1439957131, Iran;* orcid.org/0000-0003-0414-0062; Email: ahrezayan@ut.ac.ir

Authors

Ali Firoozbakhtian − *Division of Nanobiotechnology, Department of Life Sciences Engineering, Faculty of New*

Table 1. Comparison of Different Strategies of CRP Testing

reference	method of detection	linear range	LOD
Rajesh et al.[29]	FET	1−10 mg L^{-1}	0.009 mg L^{-1}
Mahyari et al.[51]	EIS	10^{-6}−0.05 mg L^{-1}	3×10^{-7} mg L^{-1}
Letchumanan et al.[17]	voltammetry	11×10^{-7}−0.11 mg L^{-1}	11.31×10^{-7} mg L^{-1}
Bryan et al.[8]	EIS	0.058−5.8 mg L^{-1}	0.019 mg L^{-1}
Magliulo et al.[65]	FET	0.046−253 mg L^{-1}	1.0 mg L^{-1}
Kim et al.[66]	FET	0.0001−0.01 mg L^{-1}	0.0001 mg L^{-1}
Vitusevich[67]	FET	5×10^{-5}−0.005 mg L^{-1}	10^{-5} mg L^{-1}
this work	FET	0.05−5 mg L^{-1}	0.017 mg L^{-1}

https://doi.org/10.1021/acsomega.1c07271
ACS Omega 2022, 7, 7341−7349

Sciences and Technologies, University of Tehran, Tehran 1439957131, Iran; orcid.org/0000-0002-3024-5258

Hassan Hajghassem − *MEMS & NEMS Laboratory, Faculty of New Sciences & Technologies, University of Tehran, Tehran 1439957131, Iran*

Fereshteh Rahimi − *Division of Nanobiotechnology, Department of Life Sciences Engineering, Faculty of New Sciences and Technologies, University of Tehran, Tehran 1439957131, Iran*

Masoud Faraghi Ghazani − *MEMS & NEMS Laboratory, Faculty of New Sciences & Technologies, University of Tehran, Tehran 1439957131, Iran*

Mahsa Kalantar − *Division of Nanobiotechnology, Department of Life Sciences Engineering, Faculty of New Sciences and Technologies, University of Tehran, Tehran 1439957131, Iran*

Amir Mohamadsharifi − *MEMS & NEMS Laboratory, Faculty of New Sciences & Technologies, University of Tehran, Tehran 1439957131, Iran*

Complete contact information is available at: https://pubs.acs.org/10.1021/acsomega.1c07271

Author Contributions

A.F.: Conceptualization, methodology, data curation, formal analysis, writing—original draft, visualization, writing—review and editing. A.H.R.: Methodology, validation, writing—review and editing, funding acquisition, project administration. H.H.: Methodology, validation, writing—review and editing, project administration. F.R.: Project administration, writing—review and editing. M.F.G.: Formal analysis, visualization. M.K.: Software. A.M.: Software.

Notes

The authors declare no competing financial interest.

■ ACKNOWLEDGMENTS

The author would like to thank the University of Tehran for funding this work.

■ REFERENCES

(1) Miller, V.; Redfield, M.; McConnell, J. Use of BNP and CRP as Biomarkers in Assessing Cardiovascular Disease:Diagnosis Versus Risk. *Curr. Vasc. Pharmacol.* **2006**, *5*, 15.

(2) Vilian, A. T. E.; Kim, W.; Park, B..; Oh, S. Y.; Kim, T. Y.; Huh, Y. S.; Hwangbo, C. K.; Han, Y. K. Efficient Electron-Mediated Electrochemical Biosensor of Gold Wire for the Rapid Detection of C-Reactive Protein: A Predictive Strategy for Heart Failure. *Biosens. Bioelectron.* **2019**, *142*, 111549.

(3) Kuo, Y.-C.; Lee, C.-K.; Lin, C.-T. Improving Sensitivity of a Miniaturized Label-Free Electrochemical Biosensor Using Zigzag Electrodes. *Biosens. Bioelectron.* **2018**, *103*, 130.

(4) Mygind, N. D.; Harutyunyan, M. J.; Mathiasen, A. B.; Ripa, R. S.; Thune, J. J.; Gøtze, J. P.; Johansen, J. S.; Kastrup, J. The Influence of Statin Treatment on the Inflammatory Biomarkers YKL-40 and HsCRP in Patients with Stable Coronary Artery Disease. *Inflammation Res.* **2011**, *60*, 281.

(5) Gabay, C.; Kushner, I. Acute-Phase Proteins and Other Systemic Responses to Inflammation. *N. Engl. J. Med.* **1999**, *340*, 448.

(6) Harbarth, S.; Holeckova, K.; Froidevaux, C.; Pittet, D.; Ricou, B.; Grau, G. E.; Vadas, L.; Pugin, J. Diagnostic Value of Procalcitonin, Interleukin-6, and Interleukin-8 in Critically Ill Patients Admitted with Suspected Sepsis. *Am. J. Respir. Crit. Care Med.* **2001**, *164*, 396.

(7) Bacli, C.; Sungurtekin, H.; Gürses, E.; Sungurtekin, U.; Kaptanoğlu, B. Usefulness of Procalcitonin for Diagnosis of Sepsis in the Intensive Care Unit. *Critical Care* **2003**, *7*, 85.

(8) Bryan, T.; Luo, X.; Bueno, P. R.; Davis, J. J. An Optimised Electrochemical Biosensor for the Label-Free Detection of C-Reactive Protein in Blood. *Biosens. Bioelectron.* **2013**, *39*, 94.

(9) Kowalczyk, A.; Sęk, J. P.; Kasprzak, A.; Poplawska, M.; Grudzinski, I. P.; Nowicka, A. M. Occlusion Phenomenon of Redox Probe by Protein as a Way of Voltammetric Detection of Non-Electroactive C-Reactive Protein. *Biosens. Bioelectron.* **2018**, *117*, 232.

(10) Simon, L.; Gauvin, F.; Amre, D. K.; Saint-Louis, P.; Lacroix, J. *Serum Procalcitonin and C-Reactive Protein Levels as Markers of Bacterial Infection: A Systematic Review and Meta-Analysis*; Clinical Infectious Diseases, 2004.

(11) Shrivastava, A. K.; Singh, H. V.; Raizada, A.; Singh, S. K. C-Reactive Protein, Inflammation and Coronary Heart Disease. *Egypt. Heart J.* **2015**, *67*, 89.

(12) Póvoa, P.; Coelho, L.; Almeida, E.; Fernandes, A.; Mealha, R.; Moreira, P.; Sabino, H. C-Reactive Protein as a Marker of Infection in Critically Ill Patients. *Clin. Microbiol. Infect.* **2005**, *11*, 101.

(13) Salminen, K.; Grönroos, P.; Eskola, J.; Nieminen, E.; Härmä, H.; Kulmala, S. Immunoassay of C-Reactive Protein by Hot Electron-Induced Electrochemiluminescence at Polystyrene-Carbon Black Composite Electrodes. *Electrochim. Acta* **2018**, *282*, 147.

(14) Lee, H.-S.; Seong, T.-Y.; Kim, W. M.; Kim, I.; Hwang, G.-W.; Lee, W. S.; Lee, K.-S. Enhanced Resolution of a Surface Plasmon Resonance Sensor Detecting C-Reactive Protein via a Bimetallic Waveguide-Coupled mode approach. *Sens. Actuators, B* **2018**, *266*, 311.

(15) Zhang, X.; Chi, K.-N.; Li, D.-L.; Deng, Y.; Ma, Y.-C.; Xu, Q.-Q.; Hu, R.; Yang, Y.-H. 2D-Porphrinic Covalent Organic Framework-Based Aptasensor with Enhanced Photoelectrochemical Response for the Detection of C-Reactive Protein. *Biosens. Bioelectron.* **2019**, *129*, 64.

(16) Pearson, T. A.; Mensah, G. A.; Hong, Y.; Smith, S. C. CDC/AHA Workshop on Markers of Inflammation and Cardiovascular Disease: Application to Clinical and Public Health Practice: Overview. *Circulation* **2004**, *110*, No. e543.

(17) Letchumanan, I.; Md Arshad, M. K.; Balakrishnan, S. R.; Gopinath, S. C. B. Gold-Nanorod Enhances Dielectric Voltammetry Detection of c-Reactive Protein: A Predictive Strategy for Cardiac Failure. *Biosens. Bioelectron.* **2019**, *130*, 40.

(18) Kitayama, Y.; Takeuchi, T. Localized Surface Plasmon Resonance Nanosensing of C-Reactive Protein with Poly(2-Methacryloyloxyethyl Phosphorylcholine)-Grafted Gold Nanoparticles Prepared by Surface-Initiated Atom Transfer Radical Polymerization. *Anal. Chem.* **2014**, *86*, 5587.

(19) Hu, W. P.; Hsu, H.-Y.; Chiou, A.; Tseng, K. Y.; Lin, H.-Y.; Chang, G. L.; Chen, S.-J. Immunodetection of Pentamer and Modified C-Reactive Protein Using Surface Plasmon Resonance Biosensing. *Biosens. Bioelectron.* **2006**, *21*, 1631.

(20) Hu, Z.; Zhou, X.; Duan, J.; Wu, X.; Wu, J..; Zhang, P..; Liang, W.; Guo, J.; Cai, H.; Sun, P.; Zhou, H..; Jiang, Z. Aptamer-Based Novel Ag-Coated Magnetic Recognition and SERS Nanotags with Interior Nanogap Biosensor for Ultrasensitive Detection of Protein Biomarker. *Sens. Actuators, B* **2021**, *334*, 129640.

(21) Lee, W.-B.; Chen, Y.-H.; Lin, H.-I.; Shiesh, S.-C.; Lee, G.-B. An Integrated Microfluidic System for Fast, Automatic Detection of C-Reactive protein. *Sens. Actuators, B* **2011**, *157*, 710.

(22) Kim, N.; Kim, D. K.; Cho, Y. J. Development of Indirect-Competitive Quartz Crystal Microbalance Immunosensor for C-Reactive protein. *Sens. Actuators, B* **2009**, *143*, 444.

(23) Wu, J.-G.; Wei, S.-C.; Luo, S.-C. In Situ Probing Unusual Protein Adsorption Behavior on Electrified Zwitterionic Conducting Polymers. *Adv. Mater. Interfaces* **2020**, *7*, 2000470.

(24) Kenaan, A.; Li, K.; Barth, I.; Johnson, S.; Song, J.; Krauss, T. F. Guided Mode Resonance Sensor for the Parallel Detection of Multiple Protein Biomarkers in Human Urine with High Sensitivity. *Biosens. Bioelectron.* **2020**, *153*, 112047.

(25) Sohrabi, H.; kholafazad Kordasht, H.; Pashazadeh-Panahi, P.; Nezhad-Mokhtari, P.; Hashemzaei, M.; Majidi, M. R.; Mosafer, J.; Oroojalian, F.; Mokhtarzadeh, A.; de la Guardia, M. Recent Advances

of Electrochemical and Optical Biosensors for Detection of C-Reactive Protein as a Major Inflammatory Biomarker. *Microchem. J.* **2020**, *158*, 105287.
(26) Centi, S.; Sanmartin, L. B.; Tombelli, S.; Palchetti, I.; Mascini, M. Detection of C Reactive Protein (CRP) in Serum by an Electrochemical Aptamer-Based Sandwich Assay. *Electroanalysis* **2009**, *21*, 1309.
(27) Sardesai, A. U.; Dhamu, V. N.; Paul, A.; Muthukumar, S.; Prasad, S. Design and Electrochemical Characterization of Spiral Electrochemical Notification Coupled Electrode (SENCE) Platform for Biosensing Application. *Micromachines* **2020**, *11*, 333.
(28) Dhara, K.; Mahapatra, D. R. Review on Electrochemical Sensing Strategies for C-Reactive Protein and Cardiac Troponin I Detection. *Microchemical Journal* **2020**, *156*, 104857.
(29) Rajesh; Sharma, V.; Puri, N. K.; Mulchandani, A.; Kotnala, R. K. High Performance Dendrimer Functionalized Single-Walled Carbon Nanotubes Field Effect Transistor Biosensor for Protein Detection. *Appl. Phys. Lett.* **2016**, *109*, 243504.
(30) Chu, C.-H.; Sarangadharan, I.; Regmi, A.; Chen, Y.-W.; Hsu, C.-P.; Chang, W.-H.; Lee, G.-Y.; Chyi, J.-I.; Chen, C.-C.; Shiesh, S.-C.; Lee, G.-B.; Wang, Y.-L. Beyond the Debye Length in High Ionic Strength Solution: Direct Protein Detection with Field-Effect Transistors (FETs) in Human Serum. *Sci. Rep.* **2017**, *7*, 5256.
(31) Sadighbayan, D.; Hasanzadeh, M.; Ghafar-Zadeh, E. Biosensing Based on Field-Effect Transistors (FET): Recent Progress and Challenges. *TrAC, Trends Anal. Chem.* **2020**, *133*, 116067.
(32) Kim, J.; Park, J. A.; Yim, G.; Jang, H.; Kim, T. H.; Sohn, H.; Lee, T. Fabrication of an Electrochemical Biosensor Composed of Multi-Functional Ag Ion Intercalated DNA Four-Way Junctions/Rhodium Nanoplate Heterolayer on a Micro-Gap for C-Reactive Protein Detection in Human Serum. *Analyst* **2021**, *146*, 2131.
(33) Lee, H. H.; Bae, M..; Jo, S. H.; Shin, J. K.; Son, D. H.; Won, C. H.; Lee, J. H. Differential-Mode HEMT-Based Biosensor for Real-Time and Label-Free Detection of C-Reactive protein. *Sens. Actuators, B* **2016**, *234*, 316.
(34) Sarangadharan, I.; Regmi, A.; Chen, Y.-W.; Hsu, C.-P.; Chen, P.-C.; Chang, W.-H.; Lee, G.-Y.; Chyi, J.-I.; Shiesh, S.-C.; Lee, G.-B.; Wang, Y.-L. High Sensitivity Cardiac Troponin I Detection in Physiological Environment Using AlGaN/GaN High Electron Mobility Transistor (HEMT) Biosensors. *Biosens. Bioelectron.* **2018**, *100*, 282.
(35) Zhao, L.; Liu, X.; Miao, B.; Gu, Z.; Wang, J.; Peng, H. X..; Zhang, J.; Zeng, B.; Li, J. A Differential Extended Gate-AlGaN/GaN HEMT Sensor for Real-Time Detection of Ionic Pollutants. *Anal. Methods* **2019**, *11*, 3981.
(36) Kim, D.-S.; Park, J.-E.; Shin, J.-K.; Kim, P. K.; Lim, G..; Shoji, S. An Extended Gate FET-Based Biosensor Integrated with a Si Microfluidic Channel for Detection of Protein complexex. *Sens. Actuators, B* **2006**, *117*, 488.
(37) Tans, S. J.; Verschueren, A. R. M.; Dekker, C. Room-Temperature Transistor Based on a Single Carbon Nanotube. *Nature* **1998**, *393*, 49.
(38) Trojanowicz, M. Analytical Applications of Carbon Nanotubes: A Review. *TrAC, Trends Anal. Chem.* **2006**, *25*, 480.
(39) Liu, A. Towards Development of Chemosensors and Biosensors with Metal-Oxide-Based Nanowires or Nanotubes. *Biosens. Bioelectron.* **2008**, *24*, 167.
(40) Kim, J. P.; Lee, B. Y.; Lee, J.; Hong, S.; Sim, S. J. Enhancement of Sensitivity and Specificity by Surface Modification of Carbon Nanotubes in Diagnosis of Prostate Cancer Based on Carbon Nanotube Field Effect Transistors. *Biosens. Bioelectron.* **2009**, *24*, 3372.
(41) Schasfoort, R. B. M.; Bergveld, P.; Kooyman, R. P. H..; Greve, J. Possibilities and Limitations of Direct Detection of Protein Charges by Means of an Immunological Field-Effect Transistor. *Anal. Chim. Acta* **1990**, *238*, 323.
(42) Justino, C. I. L.; Freitas, A. C.; Amaral, J. P.; Rocha-Santos, T. A. P.; Cardoso, S.; Duarte, A. C. Disposable Immunosensors for C-Reactive Protein Based on Carbon Nanotubes Field Effect Transistors. *Talanta* **2013**, *108*, 165.
(43) Hao, Z.; Wang, Z.; Li, Y.; Zhu, Y.; Wang, X.; De Moraes, C. G.; Pan, Y.; Zhao, X.; Lin, Q. Measurement of Cytokine Biomarkers Using an Aptamer-Based Affinity Graphene Nanosensor on a Flexible Substrate toward Wearable Applications. *Nanoscale* **2018**, *10*, 21681.
(44) Wang, X.; Zhu, Y.; Olsen, T. R.; Sun, N.; Zhang, W.; Pei, R.; Lin, Q. A Graphene Aptasensor for Biomarker Detection in Human Serum. *Electrochim. Acta* **2018**, *290*, 356.
(45) Maehashi, K.; Katsura, T.; Kerman, K.; Takamura, Y.; Matsumoto, K.; Tamiya, E. Label-Free Protein Biosensor Based on Aptamer-Modified Carbon Nanotube Field-Effect Transistors. *Anal. Chem.* **2007**, *79*, 782.
(46) Song, S.; Wang, L.; Li, J.; Fan, C.; Zhao, J. Aptamer-Based Biosensors. *TrAC, Trends Anal. Chem.* **2008**, *27*, 108.
(47) Hermann, T.; Patel, D. J. Adaptive Recognition by Nucleic Acid Aptamers. *Science* **2000**, *287*, 820.
(48) Ferreira, C. S. M.; Matthews, C. S.; Missailidis, S. DNA Aptamers That Bind to MUC1 Tumour Marker: Design and Characterization of MUC1-Binding Single-Stranded DNA Aptamers. *Tumor Biol.* **2006**, *27*, 289.
(49) Ng, E. W. M.; Shima, D. T.; Calias, P.; Cunningham, E. T.; Guyer, D. R.; Adamis, A. P. Pegaptanib, a Targeted Anti-VEGF Aptamer for Ocular Vascular Disease. *Nature Reviews Drug Discovery* **2006**, *5*, 123.
(50) Tuerk, C.; Gold, L. Systematic Evolution of Ligands by Exponential Enrichment: RNA Ligands to Bacteriophage T4 DNA Polymerase. *Science* **1990**, *249*, 505.
(51) Mahyari, M.; Hooshmand, S. E.; Sepahvand, H.; Gholami, S.; Rezayan, A. H.; Zarei, M. A. Gold Nanoparticles Anchored onto Covalent Poly Deep Eutectic Solvent Functionalized Graphene: An Electrochemical Aptasensor for the Detection of C-Reactive Protein. *Mater. Chem. Phys.* **2021**, *269*, 124730.
(52) Yaghoubi, M.; Rahimi, F.; Negahdari, B.; Rezayan, A. H.; Shafiekhani, A. A Lectin-Coupled Porous Silicon-Based Biosensor: Label-Free Optical Detection of Bacteria in a Real-Time Mode. *Sci. Rep.* **2020**, *10*, 16017.
(53) Taheri, R. A.; Rezayan, A. H.; Rahimi, F.; Mohammadnejad, J.; Kamali, M. Development of an Immunosensor Using Oriented Immobilized Anti-OmpW for Sensitive Detection of Vibrio Cholerae by Surface Plasmon Resonance. *Biosens. Bioelectron.* **2016**, *86*, 484.
(54) Bagdeli, S.; Rezayan, A. H.; Taheri, R. A.; Kamali, M.; Hosseini, M. FRET- Based Immunoassay Using CdTe and AuNPs for the Detection of OmpW Antigen of Vibrio Cholerae. *J. Lumin.* **2017**, *192*, 932.
(55) Latil, S.; Henrard, L. Charge Carriers in Few-Layer Graphene Films. *Phys. Rev. Lett.* **2006**, *97*, 036803.
(56) Lee, J.-H.; Choi, Y.-K.; Kim, H.-J.; Scheicher, R.-H.; Cho, J.-H. Physisorption of DNA Nucleobases on h -BN and Graphene: VdW-Corrected DFT Calculations. *J. Phys. Chem. C* **2013**, *117*, 13435.
(57) Mansouri Majd, S.; Salimi, A. Ultrasensitive Flexible FET-Type Aptasensor for CA 125 Cancer Marker Detection Based on Carboxylated Multiwalled Carbon Nanotubes Immobilized onto Reduced Graphene Oxide Film. *Anal. Chim. Acta* **2018**, *1000*, 273.
(58) Sigma Aldrich. IR Spectrum Table & Chart| Sigma-Aldrich. *IR Spectrum Table & Chart*, 2018; p 1.
(59) Montanheiro, T. L. D. A.; Cristóvan, F. H.; Machado, J. P. B.; Tada, D. B..; Durán, N.; Lemes, A. P. Effect of MWCNT Functionalization on Thermal and Electrical Properties of PHBV/MWCNT Nanocomposites. *J. Mater. Res.* **2014**, *30*, 55.
(60) An, J. H.; Park, S. J.; Kwon, O. S.; Bae, J.; Jang, J. High-Performance Flexible Graphene Aptasensor for Mercury Detection in Mussels. *ACS Nano* **2013**, *7*, 10563.
(61) Chen, H..; Huang, J.; Palaniappan, A.; Wang, Y.; Liedberg, B..; Platt, M.; Tok, A. I. Y. A Review on Electronic Bio-Sensing Approaches Based on Non-Antibody Recognition Elements. *Analyst* **2016**, *141*, 2335.

https://doi.org/10.1021/acsomega.1c07271
ACS Omega 2022, 7, 7341−7349

(62) Ohno, Y.; Maehashi, K.; Matsumoto, K. Label-Free Biosensors Based on Aptamer-Modified Graphene Field-Effect Transistors. *J. Am. Chem. Soc.* **2010**, *132*, 18012.
(63) Hao, Z.; Pan, Y.; Shao, W.; Lin, Q.; Zhao, X. Graphene-Based Fully Integrated Portable Nanosensing System for on-Line Detection of Cytokine Biomarkers in Saliva. *Biosens. Bioelectron.* **2019**, *134*, 16.
(64) Ohno, Y.; Maehashi, K.; Yamashiro, Y.; Matsumoto, K. Electrolyte-Gated Graphene Field-Effect Transistors for Detecting Ph and Protein Adsorption. *Nano Lett.* **2009**, *9*, 3318.
(65) Magliulo, M.; Manoli, K.; Seshadri, P.; Tiwari, A..; Torsi, L.; Liu, Z.; Zheng, L. R. A Nanotube/Polymer Composite Biosensing Thin-Film Transistor Platform for C-Reactive Protein Detection. In *IEEE-NANO 2015—15th International Conference on Nanotechnology*, 2015.
(66) Kim, C.-H.; Ahn, J.-H.; Kim, J.-Y.; Choi, J.-M.; Lim, K.-C.; Park, T. J.; Heo, N. S.; Lee, H. G.; Kim, J. W.; Choi, Y.-K. CRP Detection from Serum for Chip-Based Point-of-Care Testing System. *Biosens. Bioelectron.* **2013**, *41*, 322.
(67) Vitusevich, S. Characteristic Frequencies and Times, Signal-to-Noise Ratio and Light Illumination Studies in Nanowire FET Biosensors : Invited Paper. *IEEE Ukrainian Microwave Week, UkrMW 2020—Proceedings*, 2020.

https://doi.org/10.1021/acsomega.1c07271
ACS Omega 2022, 7, 7341−7349